International Journal for

Computational Civil and Structural Engineering

Volume 1 / Issue 2 2000

TABLE OF CONTENTS

International Journal for Computational Civil and Structural Engineering, Vol.1, pp. 46-56 (2000)

Accurate Modeling and Fast Solver for the Stress Analysis of Concrete Materials Based on the Digital Image Processing Technique

Gakuji Nagai, [1] *Takahiro Yamada,* [2] *and Akira Wada* [3]

[1] Department of Environmental Physics and Engineering, Interdisciplinary Graduate School of Science and Engineering, Tokyo Institute of Technology, Yokohama, Japan;
[2] Department of Architecture, Faculty of Engineering Science, University of Tokyo, Tokyo Japan;
[3] Structural Engineering Research Center, Tokyo Institute of Technology, Yokohama Japan.

* Address correspondence to.....

ABATRACT: This paper presents a method for the stress analysis of concrete materials. For precise simulation, concrete materials are treated as two-phase composites consisting of coarse aggregates and mortar. A set of governing equations derived from the homogenization method is used, because the elastic problem for concrete materials is a kind of multiscale problem. A three-dimensional digital image acquired from a concrete specimen is used to generate directly a geometrically accurate finite element mesh. In this case, a very large linear equation system must be solved by iterative methods with efficient preconditioners. Therefore, a procedure for digital image processing as finite element meshing is illustrated, some preconditioners based on the spectral method are described, and numerical experiments are shown.

1 INTRODUCTION

Concrete materials experience tensile failure, hence are said to be quasi-brittle. The mechanical behavior of a macroscopic structure of concrete with tensile loading has been explained by fracture mechanics based on the assumption of a homogeneous material. However, for compressive loading, it is essential to consider local tensile failures resulting from the heterogeneity of the material. To accurately model such local failures in numerical analyses, the material must be dealt with as a composite material. In this study, we assume that concrete has a two-phase structure consisting of coarse aggregates and mortar. Because of the existence of more microscopic constituents such as fine aggregates and cement paste, this two-phase structure may be approximated as a mesoscopic structure.

The homogenization method is suitable for our purpose of stress analysis. The homogenization method is categorized into the theory of multiscale analysis, and it is remarkable in the field of composite materials. In the numerical analysis of a mesoscopic structure, the geometric model must define the shapes of the coarse aggregates and their positions without any overlapping, and the corresponding finite element (FE) mesh must be generated. This procedure, especially in the three-dimensional case, results in the following problems:

1. There are too geometric modeling parameters to be defined. Even if random numbers are used, modeling accuracy is poor.
2. Coarse aggregates in the mesoscopic structure usually occupy 35 to 45% of the volume. Therefore, it is difficult for almost all the algorithms to generate a good FE mesh with the boundaries of tiled elements fitted to the interfaces between aggregates and mortar.

To overcome these problems, we adopt an alternative method of FE meshing.[1-3] This method, which requires only the sampling procedure, is the same as that for acquiring digital images. Therefore, we can use digital image processing techniques, and all the mesh generation procedures can be replaced by digital image processing. It is thus simple and easy to generate FE meshes. The original concept of this digital-image-based FE was proposed by Hollister and Kikuchi[4] in the field of biomechanics. To analyze stress in bone tissue, which has a structure too complicated to generate a conventional FE mesh, these investigators directly applied a three-dimensional digital image of bone tissue.

1524-5845/2000/$5

However, the digital-image-based FE model has a tremendous number of degrees of freedom (DOFs), and considerable time and computer resources are required to solve a linear equation discretized on a digital-image-based FE mesh. Since, however, the digital-image-based FE mesh is one of the simplest structured meshes, efficient iterative solvers may be available. One possible choice is the multigrid method, but because of the periodic domain condition in the homogenization method, we decided to use the spectral method to construct preconditioners. Glowinski et al.[5] and Tanaka et al.[6] reported that preconditioners constructed by wavelets are very efficient for the two-dimensional Laplace equation. Indeed, preconditioners must be good for three-dimensional elastic problems because the equation for elastic problems is also classified as an elliptic problem.

The rest of this article is organized as follows. Section 2 describes how a digital-image-based mesh is applicable to the stress analysis of concrete materials and illustrates the acquisition and processing of a real three-dimensional digital image. Section 3 describes a fast and efficient iterative linear equation solver. Section 4 shows some numerical results. Section 5 gives concluding remarks.

2 MODELING OF CONCRETE MATERIAL

2.1 The Homogenization Method

The formulation of the homogenization method is outlined in the following equations. For further details, see Guedes and Kikuchi.[7] Let us consider a parameter ε, which is the scale ratio of the coordinate x in a macroscopic structure to the coordinate y in a mesoscopic structure, that is,

$$\varepsilon = x/y \tag{1}$$

Take an asymptotic expansion of displacement function $u^{\varepsilon}(x)$ with respect to ε,

$$u^{\varepsilon}(x) = u^0(x,y) + \varepsilon u^1(x,y) + \varepsilon^2 u^2(x,y) + \ldots \tag{2}$$

Upon substituting equation (2) into a set of the governing equations for the elastic problem and taking a singular perturbation with respect to ε, one obtains a set of separated governing equations on different scales. The equation for the macroscopic structure is an ordinary differential equation except for the homogenized elastic modulus E^H, and a weak form of the equation for the mesoscopic structure is:

$$\int_Y E_{ijkl}(y) e^y_{kl}(\chi^{mn}) e^y_{ij}(v) dy = -\int_Y E_{ijmn}(y) e^y_{ij}(v) dy \tag{3}$$

where Y denotes a periodic domain of the mesoscopic structure, E is an elastic modulus tensor, χ is a characteristic function that associates the periodic deformation in the microscopic domain Y with the deformation in the macroscopic structure, and $e^y(\cdot)$ denotes an operator that derives infinite strain from the periodic deformation function in the mesoscopic domain Y.

The homogenized elastic modulus E^H is:

$$E^H_{ijkl} = \frac{1}{\int_Y dy} \int_Y E_{ijkl}(y)\{\delta_{km}\delta_{ln} + e^y_{kl}(\chi^{mn})\} dy \tag{4}$$

Strain and stress in the mesoscopic structures are, respectively:

$$e_{ij}(u^{\varepsilon}) = e^x_{ij}(u^0) + e^x_{ij}(\chi^{kl}) e^y_{kl}(u^0) \tag{5}$$

$$\sigma^{\varepsilon}_{ij} = E_{ijkl}\, e(u^{\varepsilon}) \tag{6}$$

2.2 An Alternative Method of Finite Element Meshing

Conventional methods of FE meshing are usually designed so that the boundaries of tiled elements are fitted to the interfaces between coarse aggregates and mortar (we refer to such arrangements as *fitted meshes*). The positions and shapes of coarse aggregates in a mesoscopic structure are so compliant that almost no algorithms could generate flexible meshes. For example, we consider the simple geometric model shown in Figure 1, in which spherical aggregates are randomly distributed. Figure 2a) shows a corresponding 20^3-divided fitted mesh, which is carefully generated by elastic deformation. It seems that there are no robust algorithms that generate fitted meshes for coarse aggregates of any shape.

Moreover, it is difficult to define the positions and shapes of aggregates. To analyze the mechanical behavior of concrete materials as composites, it is very important to generate a geometrically accurate model of the mesoscopic structure of the material. Thus, the fitted mesh has some drawbacks for modeling mesoscopic structure.

To overcome these problems, a fixed uniform grid on Cartesian coordinates is utilized as an alternative method of generating an FE mesh. The method of generating the mesh requires only sampling on the fixed grid. This procedure is found to be

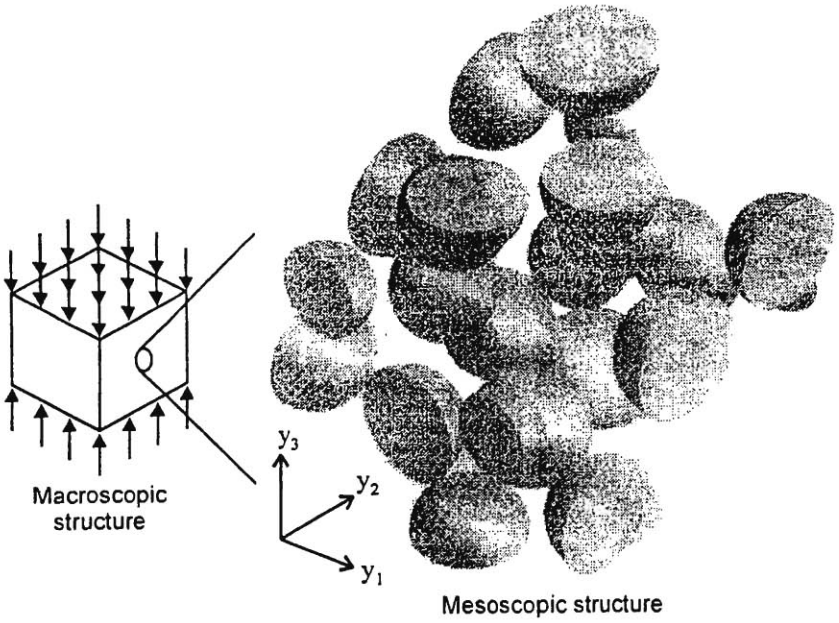

Figure 1. Randomly distributed coarse aggregates of sphere shapes.

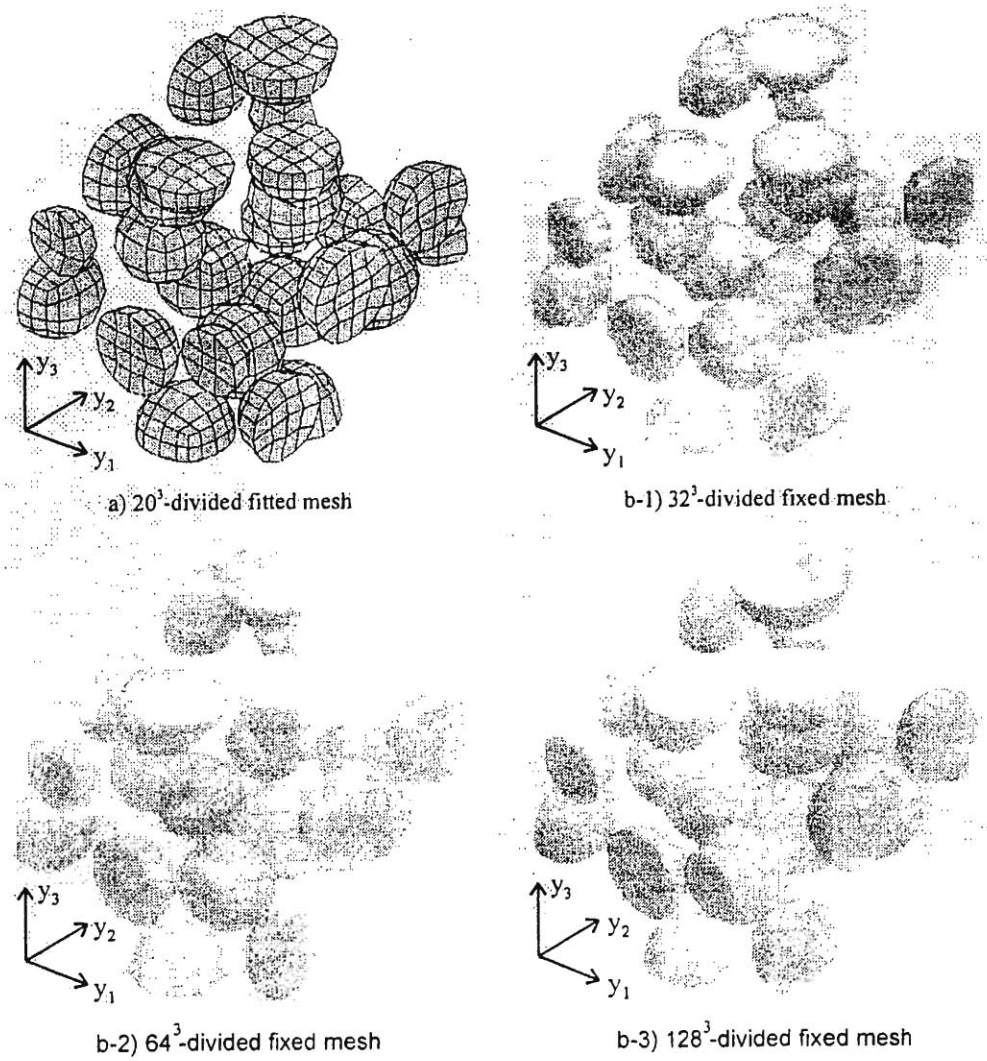

Figure 2. Comparison of FE meshing methods.

the same as the digital image procedure. In the field of digital image processing, a small element defined on a grid point is called a *voxel* (volume cell). All voxels have exactly the same cubic shape. If one voxel is regarded as one finite element, the domain can be decomposed into exactly the same shaped elements. This is referred to as a *fixed mesh.*

To compare a fixed mesh with a fitted mesh, we perform stress analyses by means of fixed meshes as shown in Figures 2b. A different sampling ratio produces fixed meshes with different numbers of mesh divisions. Stress σ_3 distributions in the y_1–y_3 centers of these meshes are shown in Figure 3. With fine mesh divisions, the fixed mesh was able to capture the mechanical behaviors of concrete materials, although it caused local numerical oscillations around the interfaces between coarse aggregates and mortar.

2.3 A Procedure for Three-Dimensional Imaging and Processing as Finite Element Meshing

A fixed mesh can be easily generated not only from models created with the assistance of computers, but also from physical objects, upon acquisition of these images. Digital images acquired from physical objects contain geometric information, and if the imaging method is appropriate, they fully reflect their geometry. We will illustrate how to acquire a three-dimensional digital image of a concrete material and how to process it to extract only geometric information.

A three-dimensional digital image can be obtained by stacking sectional two-dimensional images. Although nondestructive imaging systems such as x-ray computed tomography (CT) and magnetic resonance imaging (MRI) are available, physical destruction is the easiest way to acquire sectional images of concrete material. Repeated scraping (Figure 4) can produce a sequential set of sectional images. Accordingly, our digitizing procedure comprises repetition of the following steps: scrape a concrete specimen with a diamond scraper and acquire its sectional image by digitizing with a color flatbed scanner for PC. The concrete mix design for the specimen to

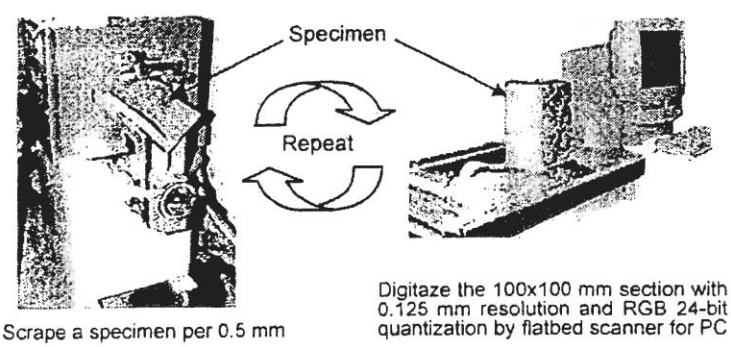

Figure 4. Acquisition of a set of sequential sectional images.

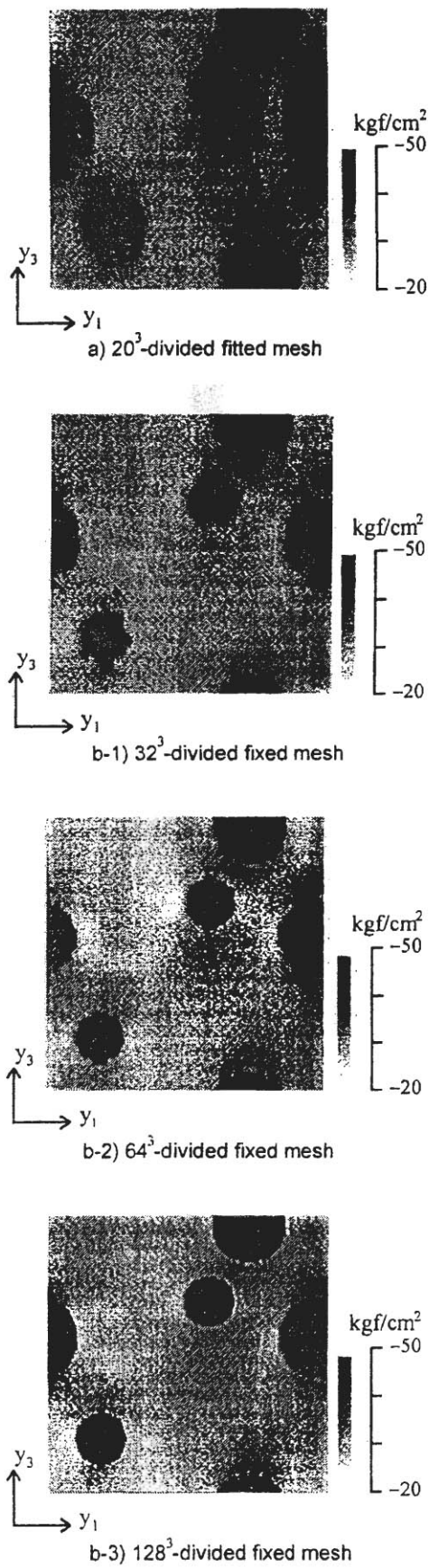

Figure 3. Comparison of stress σ_3 distribution (y_1–y_2 center section).

be destroyed is given in Table 1. The cement paste in this specimen was colored with red Fe_2O_3 pigment for easy image processing, since concrete materials are usually grayish.

Table 1. Concrete Mix Design

Cement	White Portland cement
W/C radio	55 %
Coarse aggregates	5.0–20.0 mm, 0.43 m^3/m^3
Fine aggregates	Max. 1.2 mm, 0.22 m^3/m^3
Pigment	Red Fe_2O_3, 9 % by weight

The digital image processing procedure is illustrated in Figure 5. First, the images are enhanced by converting three RGB channels into one channel. Second, binary images are made by thresholding with a certain value. The thresholding values are decided by trial and error. A binary image has sets that represent the coarse aggregates, and the complements of the sets represent the mortar. Third, fine aggregates in the mortar are eliminated from the images, because in the fixed mesh they seem to be insufficient for good resolution of physical phenomena. Additionally, fine aggregates are much smaller than coarse aggregates. Fourth, resolution of images is converted and distance images are made to interpolate among them. Fifth, the distance images are interpolated linearly and made into binary images by thresholding. Finally, upon stacking all images, a three-dimensional binary image is obtained.

3 PRECONDITIONER BASED ON SPECTRAL METHOD

Although there are relatively few sampling points in each dimension of the three-dimensional digital image described in Section 2, the total number of DOFs is tremendous. For example, a three-dimensional image represented on 256^3 sampling points has about 50 million DOFs, which requires 384 MB of memory in double precision. Section 3.1 describes how to quickly and efficiently solve this large linear equation discretized on a fixed mesh.

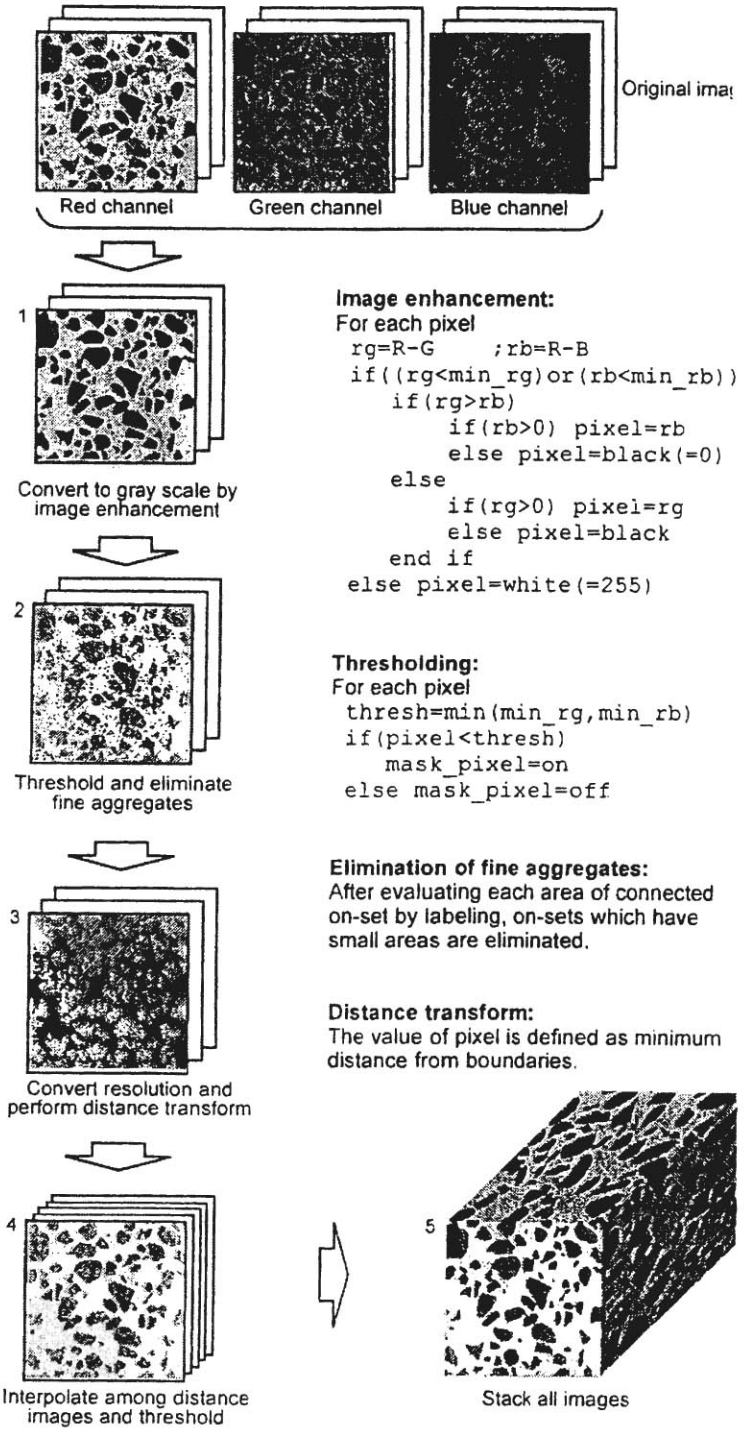

Figure 5. A procedure for image processing.

3.1 Preconditioned Conjugate Gradient Solver

Iterative methods are more suitable for solving large linear equation system than direct methods. The preconditioned conjugate gradient (PCG) method is one of the most efficient. It is well known that the method of constructing a preconditioner is the important point in minimizing the number of iterations.

Figure 6 shows the algorithm for the PCG method. The number of iterations for convergence is proportional to $\sqrt{\kappa}$, where κ is the condition number of the stiffness matrix. The increase in the number of mesh divisions makes the condition number κ wrong. In general, when the preconditioner closely approximates the exact inverse of **K**, a small number of iterations is achieved. The number of floating-point operation counts (flops) in multiplying the stiffness matrix **K** by the displacement vector **p** is about $1.152 \times L \times M \times N$ with the element-by-element method. Roughly speaking, the number of flops in applying preconditioner **M** should be less than that in multiplying part **Kp**.

Solve $\mathbf{K}\,\mathbf{x} = \mathbf{f}$

Initialize

Initial guess for $\mathbf{x}_0$

$\mathbf{r}_0 = \mathbf{f} - \mathbf{K}\,\mathbf{x}_0$

$\mathbf{p}_0 = \mathbf{z}_0 = \mathbf{M}^{-1}\mathbf{r}_0$

Iterate

$\mathbf{q}_k = \mathbf{K}\,\mathbf{p}_k$

$\alpha_k = (\mathbf{z}_k, \mathbf{r}_k)/(\mathbf{p}_k, \mathbf{q}_k)$

$\mathbf{x}_{k+1} = \mathbf{x}_k + \alpha_k \mathbf{p}_k$

$\mathbf{r}_{k+1} = \mathbf{r}_k - \alpha_k \mathbf{q}_k$

Check for convergence

$\mathbf{z}_{k+1} = \mathbf{M}^{-1}\mathbf{r}_{k+1}$

$\beta_k = (\mathbf{z}_{k+1}, \mathbf{r}_{k+1})/(\mathbf{z}_k, \mathbf{r}_k)$

$\mathbf{p}_{k+1} = \mathbf{z}_{k+1} + \beta_k \mathbf{p}_k$

Figure 6. Algorithm for PCG.

3.2 Basics of Spectral Transform

The properties of periodicity and a fixed grid in the mesoscopic structure allow us to discretize equation (2) by the spectral Galerkin methods.[8] To approximate the characteristic function χ, we choose two kinds of spectral functions whose bases are built from the one-dimensional tensor product:

1. Truncated Fourier series:

$$\chi(y_1, y_2, y_3) \cong \sum_{p=0}^{L-1} \sum_{q=0}^{M-1} \sum_{r=0}^{N-1} c_{p,q,r} \phi(y_1)\phi(y_2)\phi(y_3)$$

$$c_{0,0,0} = 0 \tag{7}$$

$$\phi(y_1) = e^{\sqrt{-1}py_1},\ \phi(y_2) = e^{\sqrt{-1}qy_2},\ \phi(y_3) = e^{\sqrt{-1}ry_3} \tag{8}$$

where (p,q,r) is a wave number set in three-dimensional space. The spatial mth derivative of $\phi(y_1)$ is:

$$\frac{d^m}{dy^m}\phi(y_1) = \left(\sqrt{-1}p\right)^m \phi(y_1) \tag{9}$$

The others are similar. The coefficients $\{c_{p,q,r}\}$ in equation (7) are solved quickly and efficiently by means of a three-dimensional real Fast fourier transform (FFT). For N data points, the number of flops for a single one-dimensional FFT is about $5/2\,N \log_2(N)$, owing to its Hermitian symmetry. Therefore, for $L \times M \times N$ three-dimensional data points, the number of flops for one three-dimensional real FFT is about $5/2\,L \times M \times N \times (\log_2(L) + \log_2(M) + \log_2(N))$. Many efficient public domain or commercial FFT libraries are available because of their wide use in the fields of physics, engineering, and signal processing. In particular, the FFTW library, which is maintained by Figro and Johnson,[9] can perform multidimensional real FFT transforms for any combination of prime numbers, although combinations of small prime numbers such as 2, 3, 5, 7, 11, and 13 are best.

2. Truncated Daubechies wavelet series:

The family of Daubechies wavelets is ordered by the number of vanishing moments DN.

With restrictions of $L = 2^l$, $M = 2^m$, and $N = 2^n$, we write

$$\chi(y_1, y_2, y_3) \cong \sum_{i}\sum_{j}\sum_{k} s_{i,j,k}^{l,m,n} \varphi_{p,i}(y_1)\varphi_{q,j}(y_2)\varphi_{r,k}(y_3)$$

$$+ \sum_{p=l}^{l}\sum_{q=l}^{m}\sum_{r=l}^{n}\sum_{i}\sum_{j}\sum_{k} d_{i,j,k}^{p,q,r} \psi_{p,i}(y_1)\psi_{q,j}(y_2)\psi_{r,k}(y_3)$$

$$s_{i,j,k}^{l,m,n} = 0 \tag{10}$$

where the pth resolution scaling function is defined as follows:

$$\varphi_{p,i}(y_1) = 2^{(l-p)/2}\varphi_{p,i}(2^{(l-p)}y_1 - i) \tag{11}$$

The pth resolution scaling function φ and the corresponding mother function ψ are given as follows:

$$\varphi_{p,i}(y_1) = \sum_{s=0}^{2DN-1} h_s \varphi_{p-1,2i+s}(y_1)$$

$$\psi_{p,i}(y_1) = \sum_{s=0}^{2DN-1} g_s \varphi_{p-1,2i+s}(y_1) \tag{12}$$

where $\{h_s\}$ and $\{g_s\}$ are Daubechies wavelet coefficients, (p,q,r) constitute a set of multiresolution approximation levels in three-dimensional wavelet space, and (i,j,k) denote dilations in each dimension with periodic domain condition. The spatial mth derivative of ψ, if it exists, is:

$$\frac{d^m}{dy_1^m}\psi_{p,i}(y_1) \cong (\psi_{p,i}(y_1))^{(m)} = 2^{(l-p)m}\psi_{p,i}^{(m)}(y_1) \tag{13}$$

The others are similar. The coefficients $\{d_{p,q,r}\}$ in equation (10) are performed quickly and efficiently by means of a three-dimensional wavelet transform (WT). For N data points, the number of flops for one a one-dimensional WT is $8\times DN\times N$ in the routine of Press et al.[10] The number of flops for one three-dimensional WT is $24\times DN\times L\times M\times N$. A more advanced wavelet theory or filter bank theory seems to be required, however, for application to data of other sizes.

Both forward and backward three-dimensional transforms are denoted by the matrix $\mathscr{C}/\mathscr{C}^{-1}$, and they are orthogonal transforms (i.e., $\mathscr{C}^{-1}=\mathscr{C}^{T}$).

3.3 Preconditioner by Means of Spectral Discretization

Upon discretizing equation (3) by either the Fourier or the wavelet Galerkin method, the following equation, expressed by matrix–vector notation, is obtained:

$$\mathbf{C}_{3\times3}^{-1}\mathbf{D}_{3\times6}\mathbf{C}_{6\times6}\mathbf{E}\,\mathbf{C}_{6\times6}^{-1}\mathbf{D}_{6\times3}\mathbf{C}_{3\times3}\,\chi^{mn}=\mathbf{f}^{mn} \tag{14}$$

where $\mathbf{f}$ is an external force vector for mode mn. Because the characteristic function vector χ has three components:

$$\chi^{mn}=\begin{Bmatrix}\chi_1^{mn}\\ \chi_2^{mn}\\ \chi_3^{mn}\end{Bmatrix} \tag{15}$$

$\mathbf{C}_{3\times3}$ and $\mathbf{C}_{3\times3}^{-1}$ are block diagonal matrices whose block diagonal elements consist of three forward andback ward three-dimensional spectral transforms $\mathscr{C}/\mathscr{C}^{-1}$, that is,

$$\mathbf{C}_{3\times3}=\begin{bmatrix}\mathscr{C}&0&0\\0&\mathscr{C}&0\\0&0&\mathscr{C}\end{bmatrix}\quad \mathbf{C}_{3\times3}^{-1}=\begin{bmatrix}\mathscr{C}^{-1}&0&0\\0&\mathscr{C}^{-1}&0\\0&0&\mathscr{C}^{-1}\end{bmatrix} \tag{16}$$

$\mathbf{C}_{6\times6}$ and $\mathbf{C}_{6\times6}^{-1}$ respectively, are similar. $\mathbf{D}$ is a block matrix that has three kinds of matrix $\mathscr{D}$ corresponding the first spatial derivative operators in spectral space. The subscript to $\mathscr{D}$ denotes a direction of the spatial derivative.

$$\mathbf{D}_{3\times6}=\begin{bmatrix}\mathscr{D}_1&0&0&\mathscr{D}_2&0&\mathscr{D}_3\\0&\mathscr{D}_2&0&\mathscr{D}_1&\mathscr{D}_3&0\\0&0&\mathscr{D}_3&0&\mathscr{D}_2&\mathscr{D}_1\end{bmatrix} \tag{17}$$

Although equation (14) could be directly applied to stress analysis, in our preliminary work, this led to wide numerical oscillations in the stress field, which were due to the stair function E.

Because we want to construct only a preconditioner, we suppose that the elastic modulus E is constant over the periodic domain Y, and we replace E with $\overline{E}$, which is spatially averaged over the periodic domain Y, that is,

$$\overline{E}_{ijkl}=\frac{1}{\int_Y dy}\int_Y E_{ijkl}\,dy \tag{18}$$

Considering equation (18), equation (14) is expressed as follows:

$$\mathbf{C}_{3\times3}^{-1}\overline{\mathbf{D}}\,\mathbf{C}_{3\times3}\chi^{mn}=\mathbf{f}^{mn} \tag{19}$$

where

$$\overline{\mathbf{D}}=\begin{bmatrix}\overline{E}_{1111}\mathscr{D}_1^2+\overline{E}_{1212}\mathscr{D}_2^2+\overline{E}_{1313}\mathscr{D}_3^2 & (\overline{E}_{1122}+\overline{E}_{1212})\mathscr{D}_1\mathscr{D}_2 & (\overline{E}_{1133}+\overline{E}_{1313})\mathscr{D}_1\mathscr{D}_3\\ (\overline{E}_{2211}+\overline{E}_{2121})\mathscr{D}_2\mathscr{D}_1 & \overline{E}_{2121}\mathscr{D}_1^2+\overline{E}_{2222}\mathscr{D}_2^2+\overline{E}_{2323}\mathscr{D}_3^2 & (\overline{E}_{2233}+\overline{E}_{2323})\mathscr{D}_2\mathscr{D}_3\\ (\overline{E}_{3311}+\overline{E}_{3131})\mathscr{D}_3\mathscr{D}_1 & (\overline{E}_{3322}+\overline{E}_{3232})\mathscr{D}_3\mathscr{D}_2 & \overline{E}_{3131}\mathscr{D}_1^2+\overline{E}_{3232}\mathscr{D}_2^2+\overline{E}_{3333}\mathscr{D}_3^2\end{bmatrix}$$

If $\mathscr{D}$ can be well approximated by a diagonal matrix, the following matrix becomes a candidate for a preconditioner:

$$\mathbf{M}=\mathbf{C}_{3\times3}^{-1}\overline{\mathbf{D}}\mathbf{C}_{3\times3} \tag{21}$$

To take the inverse of $\mathbf{M}$, six spectral three-dimensional transforms are required per iteration in PCG. Consequently, it is obvious that $\mathbf{M}$ corresponds to the following operator:

$$\begin{bmatrix}\overline{E}_{1111}\dfrac{\partial^2}{\partial y_1^2}+\overline{E}_{1212}\dfrac{\partial^2}{\partial y_2^2}+\overline{E}_{1313}\dfrac{\partial^2}{\partial y_3^2} & (\overline{E}_{1122}+\overline{E}_{1212})\dfrac{\partial^2}{\partial y_1\partial y_2} & (\overline{E}_{1133}+\overline{E}_{1313})\dfrac{\partial^2}{\partial y_1\partial y_3}\\ & \overline{E}_{1212}\dfrac{\partial^2}{\partial y_1^2}+\overline{E}_{2222}\dfrac{\partial^2}{\partial y_2^2}+\overline{E}_{2323}\dfrac{\partial^2}{\partial y_3^2} & (\overline{E}_{2233}+\overline{E}_{2323})\dfrac{\partial^2}{\partial y_2\partial y_3}\\ \text{sym} & & \overline{E}_{1313}\dfrac{\partial^2}{\partial y_1^2}+\overline{E}_{2323}\dfrac{\partial^2}{\partial y_2^2}+\overline{E}_{3333}\dfrac{\partial^2}{\partial y_3^2}\end{bmatrix} \tag{22}$$

Fast Fourier Transform

In the spectral domain, spatial derivative operators are composed of wave numbers (p,q,r) only in diagonal terms, and all nondiagonal terms are zero. Therefore, differentiation matrixes $\mathcal{D}$ are diagonal. For wave numbers (p,q,r), the components of $\overline{\mathbf{D}}$ are:

$$\overline{\mathbf{D}}_{(p,q,r)} = \tag{23}$$

$$\begin{bmatrix} \overline{E}_{1111}p^2 + \overline{E}_{1212}q^2 + \overline{E}_{1313}r^2 & (\overline{E}_{1122} + \overline{E}_{1212})pq & (\overline{E}_{1133} + \overline{E}_{1313})pr \\ & \overline{E}_{2121}p^2 + \overline{E}_{2222}q^2 + \overline{E}_{2323}r^2 & (\overline{E}_{2233} + \overline{E}_{2323})qr \\ \text{sym} & & \overline{E}_{3131}p^2 + \overline{E}_{3232}q^2 + \overline{E}_{3333}r^2 \end{bmatrix}$$

A 3×3 matrix $\mathbf{D}_{(p,q,r)}$ can be inverted easily. Because the coefficients $c_{0,0,0}$ represent rigid deformation in the periodic domain, they must be fixed. For an N^3 mesh, the flops ratio of the preconditioning part $\mathbf{M}^{-1}\mathbf{r}$ to the element-by-element multiplication part $\mathbf{Kp}$ is $1: 1/25\times\log_2(N)$. Therefore, this FFT PCG is practical for today's computer resources (at most, $N \le 2^{10}$).

Wavelet Transform

Because the differentiation matrices $\mathcal{D}$ are not diagonal but sparse, only the orders in their diagonal terms are used. Beylkin[11] and Jaffard[12] have proved that condition κ of the preconditioned stiffness matrix is suppressed within a certain number, which is independent of the number of mesh divisions. For multiresolution levels (p,q,r), the components of roughly approximated $\overline{\overline{\mathbf{D}}}$ are as follows:

$$\overline{\overline{\mathbf{D}}}^{(p,q,r)}_{(i,j,k)} = \tag{24}$$

$$\begin{bmatrix} \overline{E}_{1111}2^{2(l-p)} + \overline{E}_{1212}2^{2(m-q)} + \overline{E}_{1313}2^{2(n-r)} & (\overline{E}_{1122} + \overline{E}_{1212})2^{l-p}2^{m-p} & (\overline{E}_{1133} + \overline{E}_{1313})2^{l-p}2^{n-r} \\ & \overline{E}_{2121}2^{2(l-p)} + \overline{E}_{2222}2^{2(m-q)} + \overline{E}_{2323}2^{2(n-r)} & (\overline{E}_{2233} + \overline{E}_{2323})2^{m-q}2^{n-r} \\ \text{sym} & & \overline{E}_{3131}2^{2(l-p)} + \overline{E}_{3232}2^{2(m-q)} + \overline{E}_{3333}2^{2(n-r)} \end{bmatrix}$$

In a similar way to FFT, the 3×3 matrix $\overline{\overline{\mathbf{D}}}^{(p,q,r)}_{(i,j,k)}$ can be inverted easily, and $s^{(l,m,n)}$ must be fixed because it corresponds to the rigid deformation mode. For an N^3 mesh, the flops ratio of $\mathbf{M}^{-1}\mathbf{r}$ to $\mathbf{Kp}$ is $1: 1/8\times DN$.

Remarks. Parallel computing is required for three-dimensional analyses with digital-image-based FE mesh because of the huge number of DOFs. Fortunately, the parallel implementation of the present procedure is quite easy. Slab decomposition with respect to a certain direction is suitable for domain decomposition, when the number of processors is less than that for the slab decomposition. The multiplying part $\mathbf{Kp}$ in PCG requires a small amount of communication between processors, but the preconditioning part $\mathbf{M}^{-1}\mathbf{r}$ requires a large amount of all-to-all communication. Therefore, the preconditioning part is critical in this implementation. In the preconditioning part, a set of spectral domain dates is stored in transposed order to minimize the amount of communication. Source code is written in High Performance Fortran (HPF), which requires only the addition of some directives to normal Fortran code and no calling explicit message passing routines.

4 NUMERICAL EXPERIMENTS

4.1 Two-Dimensional Numerical Experiments on Spectral PCG Convergence

To compare the number of iterations on the spectral PCGs, numerical experiments are performed as plane strain problems. Fixed meshes for these experiments are taken from a digital image, as shown in Figure 7. The Material properties for the mortar and coarse aggregates are given in Table 2. The criterion for convergence is that the $L2$ ratio of the residual force $\mathbf{r}$ to the external force $\mathbf{f}$ must be under 10^{-6}.

Daubechies wavelets, whose vanishing moments are DN = 2,3, and 5, are chosen. Furthermore, the non-preconditioned CG and the diagonally scaled PCG are compared with spectral PCGs.

Table 2. Material Property

	Mortar	Coarse aggregates
Young's modulus, kgf/cm^2	2×10^5	5.4×10^5
Poisson's ratio	0.19	0.15

The concept of the digital-image-based FE method described in this article is the simplest one. In nonlinear analysis, some extended concept such as sub-*h* and super-*h* (*h* is the width of the crack band), which have been classified by T. Belytschko et al.,[13] may be available within the framework of the digital-image-based FE method. In our future work, we plan to analyze the nonlinear mechanical behaviors of concrete materials with discontinuous finite elements classified into sub-*h*. In sub-*h*, the geometry of the interfaces between coarse aggregates and mortar is embedded in finite elements with hierarchical images. With these finite elements, no local oscillations would appear near the interfaces in stress field.

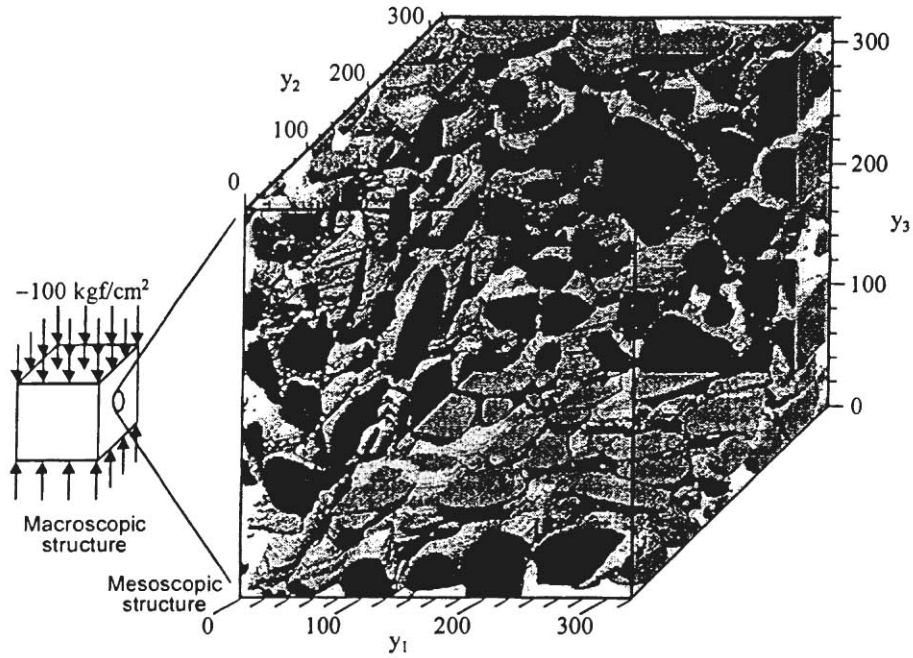

Figure 9. A 320^3-divided fixed mesh model.

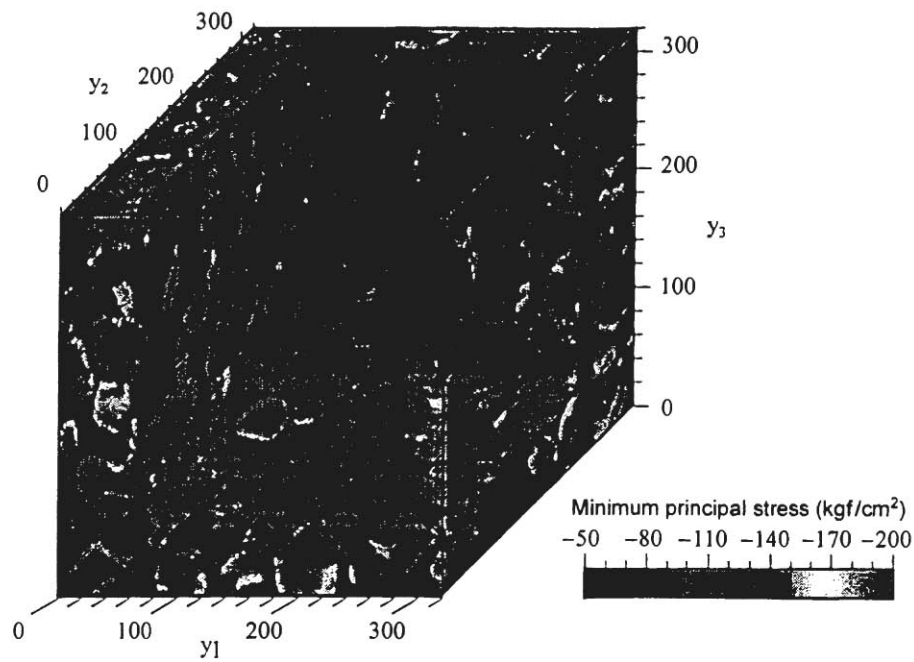

Figure 10. Minimum principal stress distribution.

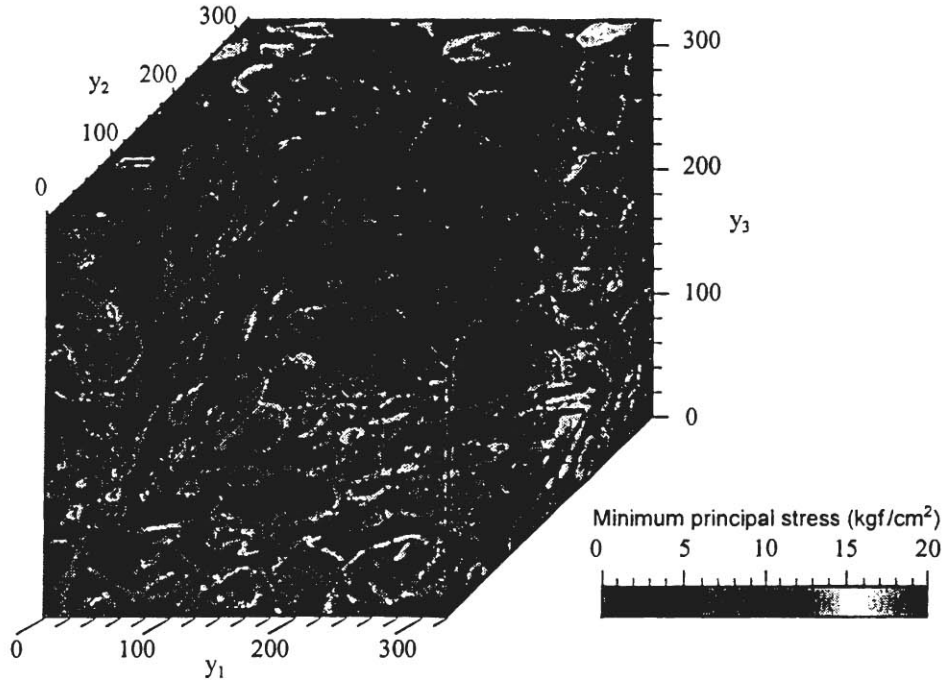

Figure 11. Maximum principal stress distribution.

ACKNOWLEDGMENTS

The first author is grateful for the financial support provided by the Takenaka Scholarship Foundation and the Research Fellowships of the Japan Society for the Promotion of Science for Young Scientists.

REFERENCES

1. G. Nagai, T. Yamada, and A. Wada. On a finite element procedure based on the real 3-dimensional image for concrete materials (in Japanese). *J. Struct. Const. Eng. (Trans. AIJ)*, **509**: 77–82, 1998.
2. G. Nagai, T. Yamada, and A. Wada. Finite element analysis of concrete material based on the 3-dimensional real image data. Presented at the Fourth World Congress on Computational Mechanics, Buenos Aires, 1998.
3. G. Nagai, T. Yamada, and A. Wada. Stress analysis of concrete material based on geometrically accurate finite element modeling. In *Fracture Mechanics of Concrete Structures, Proceedigs of FRAMCOS-3*, H. Mihashi and K. Rokugo, eds.: AEDIFICATIO Publishers, 1998, pp. 1077–1086.
4. S. J. Hollister and N. Kikuchi. Homogenization theory and digital imaging: A basis for studying the mechanics and design principles of bone tissue. *Biotechnol. Bioeng.* **43**: 586–596, 1994.
5. R. Glowinski, A. Rieder, R. O. Wells, and X. Zhou. A wavelet multigrid preconditioner for Dirichlet boundary-value problems in general domains. Preprint, 1994.
6. N. Tanaka, H. Terasaka, T. Shimizu, and Y. Takigawa. Incomplete discrete wavelet transform and its application to a Poisson equation solver. *J. Nucl. Sci. Technol.* **33**(7): 555–561, 1996.
7. G. M. Guedes and N. Kikuchi. Preprocessing and postprocessing for materials based on the homogenization method with adaptive finite element methods. *Comput. Methods Appl. Mech. Eng.* **83**: 143–198, 1990.
8. C. Canuto, M. Y. Hussaini, A. Quarteroni, and T. A. Zang. *Spectral Methods in Fluid Dynamics*. New York: Springer-Verlag, 1998.
9. M. Frigo and S. G. Johnson. FFTW User's Manual for version 2.0, 1998. *http://theory.lcs.mit.edu/-fftw/*
10. W. H. Press, S. A. Teukolsky, W. T. Vetterling, and B. P. Flannery. *Numerical Recipes in FORTRAN: The Art of Scientific Computing*, 2nd ed. Cambridge: Cambridge University Press, 1992.
11. G. Beylkin. On the representation of operators in bases of compactly supported wavelets. *SIAM J. Numer. Anal.* 6(6): 1716–1740, 1992.
12. Jaffard
13. T. Belytschko, J. Fish, and B. E. Engelmann. A finite element with embedded localization zones. *Comput. Methods Appl. Mech. Eng.* **70**: 59–89, 1988.